

1 **Falkland Island peatland development** 2 **processes and the pervasive presence of** 3 **fire**

4

5 Dmitri Mauquoy^{1#}, Richard J Payne^{2*}, Kirill V. Babeshko³, Rebecca Bartlett⁴, Ian
6 Boomer⁴, Hannah Bowey¹, Chris D. Evans⁵, Fin Ring-Hrubesh², David Muirhead¹,
7 Matthew O'Callaghan⁴, Natalia Piotrowska⁶, Graham Rush², Thomas Sloan², Craig
8 Smeaton⁷, Andrey N. Tsyganov^{8,9}, Yuri A. Mazei^{8,9}

9

- 10 1. Geography and Environment, School of Geosciences, University of
11 Aberdeen, St Mary's Building, Aberdeen AB24 3UF, United Kingdom
- 12 2. Environment and Geography, University of York, York YO10 5NG, United
13 Kingdom
- 14 3. Department of Zoology and Ecology, Penza State University, 440026, Penza,
15 Russia
- 16 4. School of Geography, Earth and Environmental Sciences, University of
17 Birmingham, Edgbaston, Birmingham B15 2TT, United Kingdom
- 18 5. Centre for Ecology & Hydrology, Environment Centre Wales, Deiniol Road,
19 Bangor, Gwynedd LL57 2UW, United Kingdom
- 20 6. Silesian University of Technology, Institute of Physics-CSE, Gliwice, Poland.
- 21 7. School of Geography & Sustainable Development, University of St Andrews,
22 St Andrews, KY16 9AL, UK
- 23 8. Department of General Ecology and Hydrobiology, Lomonosov Moscow State
24 University, 119991, Moscow, Russia
- 25 9. A.N. Severtsov Institute of Ecology and Evolution RAS, 119071, Moscow,
26 Russia

27 #Corresponding author, d.mauguoy@abdn.ac.uk

28 *Deceased

29

30 *Abstract*

31

32 Palaeoecological analyses of Falkland Island peat profiles have largely been
33 confined to pollen analyses. In order to improve understanding of long-term Falkland
34 Island peat development processes, the plant macrofossil and stable isotope
35 stratigraphy of an 11,550 year Falkland Island *Cortaderia pilosa* ('whitegrass') peat
36 profile was investigated. The peatland developed into an acid, whitegrass peatland
37 via a poor fen stage. Macrofossil charcoal indicate that local fires have frequently
38 occurred throughout the development of the peatland. Raman spectroscopy analyses
39 indicate changes in the intensity of burning which are likely to be related to changes
40 in fuel types, abundance of fine fuels due to reduced evapotranspiration/higher
41 rainfall (under weaker Southern Westerly Winds), peat moisture and human
42 disturbance. Stable isotope and thermogravimetric analyses were used to identify a
43 period of enhanced decomposition of the peat matrices dating from ~7020 cal yr BP,
44 which possibly reflects increasing strength of the Southern Westerly winds. The
45 application of Raman spectroscopy and thermogravimetric analyses to the Falkland
46 Island peat profile identified changes in fire intensity and decomposition which were
47 not detectable using the techniques of macrofossil charcoal and plant macrofossil
48 analyses.

49

50 Keywords: Holocene; Southern Westerly Winds; Fire; Vegetation Dynamics; Falkland
51 Islands; Raman Spectroscopy; Thermogravimetric Analysis; Testate Amoebae;
52 Charcoal

53

54 *1 Introduction*

55

56 The Falkland Islands cover an area of approximately 12,200 km² and peatlands there
57 comprise ~40-50% of the total land area (pers. comm. Matt Aitkenhead). The
58 estimated carbon stock of peatlands in the archipelago is ~156 MtC (Payne et al.,
59 2019). The earliest peat deposits date to ~16,500 cal yr years BP (Wilson et al.,
60 2002), therefore Falkland Islands peat deposits have the potential to give insight into
61 long-term carbon processing and storage. They also have the potential to provide
62 palaeoclimate data in order to understand the long-term variability of the Southern
63 Westerly Winds (SWW), given that they lie within the main latitudinal belt (52°S) of
64 the Southern Hemisphere westerly airflow and westerly wind days in the Falkland
65 Islands are the most dominant, with an average of ~180 days per year (Jones et al.,
66 2016). Based upon ERA-79 Interim reanalysis data (1979-2013 CE), there is a
67 positive correlation between the hemispherically averaged Southern Annular Mode
68 (SAM) index and 2–10 m air temperature and wind strength in the Falkland Islands
69 (Turney et al., 2016).

70 Palaeoclimate data generated from peat profiles in the Falkland Islands can
71 potentially complement the extensive research which has been undertaken in
72 southern South America to detect variability of the SWW (Kilian and Lamy, 2012).
73 However, there are some potential caveats to this, as Falkland Island peat
74 accumulation rates appear to be highly variable which potentially limits their temporal
75 resolution. Payne et al. (2019) recorded low to very low, long-term apparent rates of
76 carbon accumulation in 10 peat profiles collected from the Falkland Islands. This
77 could be due to low initial rates of carbon accumulation or be a consequence of
78 subsequent carbon loss.

79 Human and associated livestock impacts on the Falkland peats, although now
80 substantial, are limited to the last 250 years; prior to the introduction of cattle, and
81 more recently sheep, there were no native grazing mammals on the islands
82 (Armstrong, 1994). Currently, very little is known about Falkland Island peatland

83 development processes. This is a necessary prerequisite for any peat-based proxy-
84 climate reconstruction, given that peatland autogenic successional changes through
85 time (Hughes et al., 2000) are not solely dependent upon allogenic (climate) forcing.

86

87 1.1 Existing palaeoecological reconstructions

88

89 A small number of Lateglacial plant macrofossils were identified in peat samples
90 collected from the Lake Sullivan (West Falkland) fan delta (Wilson et al., 2002), but
91 their analysis was not systematically undertaken in the peat deposits investigated. To
92 date only a single, detailed charcoal and plant macrofossil record is available from
93 the Falkland Islands (Hooker's Point), spanning the Pleistocene/Holocene transition
94 (Scaife et al., 2019).

95 The few palaeoecological reconstructions which have been undertaken in the
96 Falkland Islands have primarily focussed upon the analyses of microfossil pollen,
97 spores and charcoal (Barrow, 1978; Clark et al., 1998; Turney et al., 2016).

98 Palaeoclimate reconstructions based upon changes in Falkland Island pollen spectra
99 have proven to be challenging due to the "...restricted vascular flora, which greatly
100 limits the amount of pollen with climatically diagnostic value" (Clark et al., 1998). To
101 circumvent problems with the low palynological diversity of the indigenous flora (high
102 dominance of *Poaceae* and *Empetrum*), changes in the concentrations of 'exotic',
103 long distance, wind dispersed *Nothofagus*, *Podocarpus*, *Ephedra fragilis* and
104 *Anacardium*-type pollen from southernmost South America (~500 km to the west)
105 have been used as a surrogate for changes in the strength of the SWW (Turney et
106 al., 2016). This same logic was also applied to microfossil charcoal (<106 µm)
107 spectra in the investigated peat profile, given that these too can be transported long
108 distances by the prevailing SWW (Clark, 1988), and potentially offer an indirect
109 measure of past airflow. The 90 cm depth Falkland Island peat profile sequence at

110 Canopus Hill investigated by Turney et al. (2016) spans the last ~2600 years and a
111 correspondence between microfossil charcoal and *Nothofagus* pollen counts was
112 noted. Both were therefore used as a proxy for long distance transport of these
113 microfossils by stronger SWW winds. Stronger westerly wind flow was identified at
114 2400, 2100, 1800–1300, 1000, 550 and 250 cal yr BP.

115 Away from the Falkland Islands, a long period of weaker SWW winds between 8300-
116 4000 cal yr BP was identified in a multi-proxy lake record from eastern Patagonia,
117 ~700 km to the SWW, followed by a re-intensification of the SWW since 3000 cal yr
118 BP (Zolitschka et al., 2019). Conversely, the diatom and ostracod data from Lake
119 Aturo in the semiarid steppe of northern Tierra del Fuego, recorded an increase of
120 salinity with sodium dominated waters due to stronger SWW between 7260-6200 cal
121 yr BP (Fernández et al., 2020).

122 Based upon the influx of aeolian sand to a peat deposit on Isla de los Estados,
123 easternmost Tierra del Fuego, Björck et al. (2012) identified a period of maximum
124 Holocene SWW strength between 4500-3500 cal yr BP.

125 Few macrofossil charcoal analyses have been undertaken in the Falkland Islands,
126 but the results of Buckland and Edwards (1998) are noteworthy, in that the basal 50
127 cm of a peat profile from Sapper Hill, East Falkland contained abundant macrofossil
128 charcoal fragments which were dated to before ~5640-5304 cal yr BP.

129 The transport distance of macrofossil charcoal is relatively low and can range
130 between several hundreds of metres (Clark et al., 1998; Blackford, 2000; Peters and
131 Higuera, 2007) to tens of kilometers from the depositional archive deposit (Pisaric,
132 2002; Tinner et al., 2006). The evidence presented by Buckland and Edwards (1998)
133 for *in situ*/local burning of the peat-forming vegetation (*Empetrum rubrum* Vahl ex
134 Willd.) is millennia before the arrival of Europeans (the first French settlement at Port
135 Louis on East Falkland dates to 1764 CE; Armstrong, 1994). The question still
136 remains whether this burning reflects the presence of pre-European humans
137 (travelling from southern South America, either by design or accident?) or natural

138 ignition through lightning strikes, given the relatively low rainfall combined with high
139 flammability of *E. rubrum*, as noted by Hooker (1847), “The stems and leafy
140 branches are much used for fuel in the Falklands where the plant is called “diddle
141 dee”, they are especially employed in kindling fire for even when sodden with rain
142 they speedily ignite and burn with a bright and hot flame”.

143 The late Quaternary fire history of Patagonia and Tierra del Fuego has been
144 reviewed by Huber et al. (2004). The microfossil charcoals identified in Torres del
145 Paine by Heusser (1995) and in Meseta Latorre I by Schäbitz (1991) both record
146 high fire activity during the entire Holocene. Both of these sites are located in xeric
147 habitats of the steppe-forest ecotone and climatic conditions in these locations during
148 the Holocene “may have always promoted fires” (Huber et al. (2004).

149 The relationship between ‘unplanned’ fires (including human and lightning ignited
150 fires) in Australia, South Africa and South America and the main Southern
151 Hemisphere climate modes, was explored by Mariani et al. (2018). Based upon these
152 documentary fire records spanning 1958-2014 CE, the Southern Annular Mode
153 (SAM) was identified as the leading climate mode in most of the analysed regions
154 across the Southern Hemisphere. Positive (southward shifted) SAM states were
155 found to be associated with a large increase in the number of fires during the 21st
156 century.

157 The impacts of burning upon the local peat forming vegetation of Falkland Island
158 peatlands is uncertain, although it is likely that pre-fire weather, peat moisture, water
159 table depth, fuel type and microtopographic position will influence the susceptibility of
160 peat to burning (Bourgeau et al., 2020).

161 In terms of fire weather, 14 discrete fires on the Falkland Islands were started by
162 lightning strikes between 2000 to 2015 CE, i.e. about one per year on average,
163 although in several cases multiple separate fires were started by a single storm. All
164 lightning strike induced fires occurred between December and April, with most of
165 them in January (Falkland Fire Service data provided by Jim McAdam, pers. comm.).

166 The effect of lowered water table depth and the vulnerability of northern peatlands to
167 burning was investigated by Turetsky et al. (2011), based upon a long-term peatland
168 drainage experiment in Canada. Carbon losses were found to be nine times higher in
169 the drained plots compared to the pristine plots. In *Sphagnum*-dominated boreal
170 peatlands, accumulation rates decrease significantly with increasing fire frequencies
171 (Kuhry, 1994). The effect of fires in boreal bogs is spatially heterogeneous and
172 dependent upon the microtopographic position (Benscoter et al., 2011). In the
173 blanket bogs of the Falklands, which lack extensive *Sphagnum* cover or typical
174 hummock-hollow microtopography, other factors such as the presence or absence of
175 fire-prone *Empetrum rubrum* (which may in turn reflect peat wetness) could have a
176 greater influence on the spatial development and severity of fires.

177

178 *1.2 Raman spectroscopy and thermogravimetric analysis*

179

180 Raman spectroscopy of organic material is a rapid, non-destructive and cost-efficient
181 technique for establishing the thermal maturity of carbonaceous materials. Raman
182 spectroscopy is based upon “Raman scattering” which is due to various elementary
183 excitations where the energy is lost or gained during the scattering process. Given
184 this, Raman spectra can be used as a “fingerprint” for different materials. Analysis of
185 Raman spectra in carbonaceous materials is used to derive the level of thermal
186 maturation of a sample and therefore has the potential to highlight the degree of
187 burning intensity in peatlands. Fossil carbonaceous materials undergo a complex
188 series of reactions when thermally altered, which involve both the formation and
189 reordering of aromatic sub-units towards stacked layers such as graphite. Raman
190 spectroscopy has been widely used (Tuinstra and Koenig 1970; Landis 1971;
191 Nemanich and Solin 1979; Knight and White 1989; Ferrari and Robertson 2001;
192 Beyssac et al. 2002; Muirhead et al., 2012; Muirhead et al., 2017; Muirhead et al.,

193 2019) as a powerful tool for evaluating the character and thermal alteration of diverse
194 forms of carbonaceous matter (crystalline, nanocrystalline, amorphous).
195 Measurement of spectroscopic parameters are mainly based on two broad first order
196 Raman bands (spectral peaks) at $\sim 1585\text{ cm}^{-1}$ (the graphite peak, G) and $\sim 1350\text{ cm}^{-1}$
197 (the disorder peak, D). A number of Raman parameters have been developed over
198 the past few decades which involve measurements made on Raman spectral peaks,
199 for example the D/G-peak ratio (I_D/I_G (Intensity [peak height])). Plotting of this ratio can
200 reveal differences in the thermal alteration of the carbonaceous materials (Pasteris
201 and Wopenka, 1991; Jehlička, and Bény 1992). There is agreement that the main
202 changes in the Raman spectra of low maturity organic matter exhibit a narrowing of
203 the G band and an increase of the D band area with thermal maturity increase.
204 Heating experiments based upon Japanese cedar wood and bark charcoal show that
205 the D-band position and the G-band width is dependent upon heat treatment
206 temperature in the region of $400^\circ\text{--}800^\circ\text{C}$ (Yamauchi and Kurimoto, 2003).
207
208 Thermogravimetric analysis (TGA) can be viewed as both a complex version of loss-
209 on-ignition (LOI, (Dean, 1974; Bengtsson and Enell, 1986)) and a more generic
210 version of rock-eval (Gregorich et al., 2015) and Ramped Pyrolysis (Rosenheim et
211 al., 2008; Rosenheim and Galy, 2012). TGA is a thermal analysis technique in which
212 the mass of a sample is measured over time as temperature ramps upwards at a
213 known rate. TGA is a measure of the whole sample composition. It is not selective
214 and does not require extraction or treatment prior to analysis, unlike other methods
215 such as biomarkers. TGA provides an analytical approach to characterise organic
216 matter (OM) providing information on the quantity, quality and reactivity of the
217 organic fraction. Through the ramped heating process the quality and reactivity of the
218 OM can be determined, in the simplest terms the labile, recalcitrant and refractory
219 components of the OM can be quantified (Capel et al., 2006) and subsequently the
220 biodegradability of the OM can be assessed (Kristensen, 1990).

221

222 1.3 Our approach

223

224 In this study we apply a suite of established and emerging palaeoecological
225 techniques to a Falkland Island peat profile to determine peatland successional
226 processes through plant macrofossil analysis and to identify whether disturbance
227 through burning is commonplace through the analysis of macrofossil charcoal. We
228 explore the potential of Raman spectroscopy as a technique to identify burning
229 intensity of subfossil char fragments, and TGA to characterise OM preserved in the
230 peat matrices following Lopez-Capel et al. (2005), Plante et al. (2009) and Worrall et
231 al. (2017). Raman spectroscopy has been applied to charcoal deposits preserved in
232 soils (Inoue et al., 2017), but as far as we are aware, has not yet been undertaken on
233 charcoal deposits preserved in peat bogs. TGA has been used to understand the
234 contemporary carbon budget of a blanket peatland (Worrall et al., 2017), but has not
235 yet been systematically applied to peat profile samples in order to identify changes in
236 decomposition through time.

237

238 In order to trace precipitation delivery by the SWW we attempt to reconstruct mire
239 surface wetness using testate amoeba assemblages and $\delta^{13}\text{C}$ in addition to the plant
240 macrofossil analyses. Testate amoebae are a group of amoeboid protists which
241 produce morphologically distinct shells and are commonly used as surface-moisture
242 proxies in peat-based palaeoclimate studies (Chambers et al., 2012). Changes in
243 testate amoebae assemblages from Tierra del Fuego and southern Patagonia have
244 been used to reconstruct changes in peatbog water table depths on raised
245 *Sphagnum magellanicum* bogs (van Bellen et al., 2016), so there is a possibility that
246 this technique may also provide insight into water table depth changes in Falkland
247 Island peat archive deposits.

248

249 2 Materials and methods

250

251 The Falkland Island blanket peatlands mainly comprise acid grasslands dominated
252 by *Cortaderia pilosa* (d'Urv.) Hack. and *Empetrum rubrum* dwarf shrub heath
253 (McAdam and Upson, 2012). Cushion (*Astelia pumila* (Forst. f.) Gaudich. and
254 bryophyte bogs (with small patches of *Sphagnum magellanicum* Brid. and *S.*
255 *fimbriatum* Wilson) are also present within the archipelago, along with the tall
256 tussock-forming tussac grass (*Poa flabellata* (Lam.) Raspail) in ungrazed coastal
257 areas and offshore islands. Falkland peatlands occupy an unusual climatic niche in
258 comparison to Northern Hemisphere peatlands (Loisel and Yu, 2013), with relatively
259 low annual precipitation (~400-600 mm) and temperate conditions with low
260 temperature variability (the mean annual temperature is ~6°C), providing long
261 growing season conditions for the local peat-forming vegetation (Payne et al., 2019).

262

263 A 211 cm length peat profile was recovered in 2018 from a whitegrass (*Cortaderia*
264 *pilosa*) dominated peatland in the Sussex mountains (SSX, 51.63278°S
265 58.99654°W,) on East Falkland (Fig. 1) using a Russian-pattern peat corer (Aaby
266 and Digerfeldt, 1986). The site is a raised (ombrotrophic) peat dome surrounded by
267 shallow whitegrass peat. The dome of peat is approximately 20 m wide along the E-
268 W axis and 30 m along the N-S axis. There is no erosion along the site margins
269 although a small crescent shape feature on the NW side is perhaps a revegetated
270 erosion scar. Probing indicated similar peat depth throughout and a core was taken
271 from near the point of highest elevation. The upper peat was notably darkly coloured
272 and highly humified. The landscape is fenced pasture land and the site is used for
273 grazing with sheep faeces noted. The nearest fence is c.100 m from the site to the
274 west and a road lies c.100 m to the east. When the peat profile was collected, the
275 peat surface was notably dry with some bare ground. The dominant plant is *E.*

276 *rubrum* with *Carex pilosa* Scop., *Blechnum penna-marina* (Poir.) Kuhn, small
277 hummocks of *Bolax gummifera* (Lam.) Sprengel (Balsam Bog), *Myrteola nummularia*
278 (Poir.) O. Berg, *Marsippospermum grandiflorum* (L.f.) Hook. and some *Cladonia* spp.
279 lichens. A total of 43 samples were available for macrofossil analysis from the 211
280 cm length SSX peat profile. These were warmed in 8% NaOH and sieved (mesh
281 diameter 180 μm). Macrofossils were identified using a binocular microscope ($\times 10$ –
282 $\times 50$) based upon modern type material collected during fieldwork. Identifications
283 were also made with reference to Michaelis (2011) for *Sphagnum* mosses. Volume
284 abundances of all components are expressed as percentages with the exception of
285 fungal fruit bodies, *Carex* spp. nutlets, *Juncus scheuchzerioides* Gaudich. seeds,
286 Acarid mites and macrofossil charcoal fragments, which are presented as the
287 number (n) found in each of the $\sim 5 \text{ cm}^3$ subsamples. Zonation of the macrofossil
288 diagram was made using psimpoll 4.27 (Bennett, 1996), using the optimal splitting by
289 information content option for the LOI, plant macrofossil and macrofossil charcoal
290 data.

291

292 Five samples were prepared for AMS ^{14}C dating using an acid-base-acid protocol
293 (Piotrowska, 2013). Samples were disaggregated and inspected under low-powered
294 microscopy before being prepared for AMS ^{14}C dating. The composition of the
295 samples and the ^{14}C dating results after calibration with the SHCal13 calibration
296 curve (Hogg et al., 2013) are presented in Table 1. Chronologies were modelled
297 using a Bayesian approach implemented in the Bacon version 2.3.9.1 package in R
298 (Blaauw and Christen, 2011). In addition, the sampling year 2018 CE was assigned
299 to the surface of the core. After calibration, the modelling procedure of Bacon takes
300 account of the entire probability distribution of each dated level while creating robust
301 chronologies including estimations of age uncertainties. The results of the Bacon
302 derived ^{14}C age/depth modelling are presented in Figure 2.

303

304 Sub-samples of ~2 cm³ volume were ground and incinerated at 550 °C to calculate
305 LOI. Separate samples for TGA were dried, milled and 20 mg of sample was placed
306 into 70 µl aluminium oxide crucibles. The crucibles were placed into a Mettler Toledo
307 TGA2 (at the University of St Andrews) and heated from 40 to 1000°C at a ramp rate
308 of 10°C min⁻¹ under a stream of N₂. The TGA traces were adjusted to be on a
309 common temperature scale and clipped to the range 150 to 650°C to remove
310 interference from absorbed water and inorganic carbon. The TGA traces were
311 normalized to the mass loss, so that all traces were on the same scale and the first
312 derivative of the TGA was calculated (DTG). Finally, the continuous OM mass loss
313 data were grouped into three thermal fractions indicative of OM lability or
314 biodegradability (Capel et al., 2006). These fractions are defined as labile (200-
315 400°C), recalcitrant (400-550°C) and refractory (550-650°C).

316

317 For δ¹³C analysis, dried samples of bulk sediment were ground to powder, then
318 subsamples of approximately 0.4-0.6 mg were weighed into tin cups and combusted
319 in an Elementar Pyrocube at 920°C. The resulting CO₂ was analysed on an Isoprime
320 Isotope Ratio Mass Spectrometer at the University of Birmingham, Geological Mass
321 Spectrometry Laboratory (GEMS). Internal precision for δ¹³C was 0.08 ‰. All
322 samples were replicated with the mean difference between replicates being
323 approximately 0.10 ‰ (range 0.242-0.005 ‰).

324

325 Testate amoebae were prepared following the method based on suspension in
326 water, physical agitation and subsequent sedimentation (Mazei and Chernyshov,
327 2011). The samples were soaked in distilled water for 24 h, agitated on a flask
328 shaker for 30 min, sieved and washed through a 500 µm mesh to remove coarse
329 material and then left to settle for 24 h. The supernatant was decanted away and the
330 samples were mixed with neutralized formaldehyde and placed in glass vials for

331 storage. One milliliter of the concentrated sample was placed in a Petri dish (5 cm
332 diameter), diluted with deionized water if necessary and inspected at $\times 200$
333 magnification.
334
335 Raman measurements of macrofossil charcoal fragments from seven samples (206,
336 181, 131, 101, 76, 46 and 16 cm core depth) were performed on a Renishaw inVia
337 reflex Raman spectrometer at the University of Aberdeen. Charcoal fragments were
338 picked from the treated macrofossil samples (warmed in 8% NaOH and sieved
339 (mesh diameter 180 μm)) using fine forceps and placed onto a slide. A Leica DMLM
340 reflected light microscope was used to focus the Ar⁺ green laser (wavelength 514.5
341 nm) on 24 different charcoal fragments from each of the samples. The laser spot size
342 was approximately 1-2 μm and laser power between 10-50% (<13 mW power at the
343 sample). The scattered light was dispersed and recorded by means of a CCD
344 (Charge Coupled Device) detector. Data were collected between 1100 cm^{-1} and 1700
345 cm^{-1} with a spectral resolution less than 3 cm^{-1} . The duration of accumulations was
346 typically up to 10 seconds for between 3 and 5 accumulations. The Renishaw WiRE
347 3.0 curve-fit software was used for spectral deconvolution. Smoothing and baseline
348 extractions were performed on each sample, including a cubic spline interpolation.
349 Each sample was deconvolved and data extracted at least three times to ensure
350 reproducibility and the removal of any background signal. Peak position and peak full
351 width at half maximum (FWHM) are measured in wavenumbers (cm^{-1}), which records
352 the change in vibrational frequency (stretching and breathing) of the Raman-active
353 carbon molecules. Minimal spectral processing and deconvolution was applied to the
354 measurement of peak areas, with composite G and D bands used to calculate I_D/I_G
355 ratios as outlined in Muirhead et al., (2012; 2017). Prior to analysis of deconvolved
356 spectra, an initial visual approach to spectral interpretation was adopted.

357

358 *3 Results and interpretation of the proxy data*

359

360 The degree of preservation of plant macrofossils in the SSX profile is relatively good
361 overall and the entire profile is dominated by undifferentiated graminoids and
362 undifferentiated graminoid roots (Fig. 3, Table 2). Only a very small proportion of the
363 graminoid macrofossils were identifiable to species level (e.g. *Cortaderia pilosa* in
364 zone SSX-5). Relatively low LOI values between 211-206 cm in zone SSX-1 (55%
365 and 67%) indicate the possible in-wash of sediments. The presence of *Carex* spp.
366 nutlets, *Juncus scheuchzerioides* seeds and *Sphagnum magellanicum* leaves and
367 stems in zone SSX-1 (~11,550-8840 cal yr BP) indicate relatively wet and poor-fen
368 conditions (intermediate between fen and bog) during the initial stages of peatland
369 development. Macrofossil charcoal fragments are frequent throughout the peat
370 profile, but relatively low numbers of charcoal fragments were identified in zone SSX-
371 3 (~6590-5470 cal yr BP). The large increase in the amount of unidentifiable organic
372 material in zone SSX-5 (~2820 cal yr BP to the present) suggests that these peat
373 samples are the most decomposed of the entire peat profile.

374

375 The preservation of testate amoebae was low with most of the samples recording
376 <10 specimens, with the exception of the samples at depths of 20 cm, 15 cm, 5 cm
377 and the surface sample, where 100+ specimens were identified. A total of 21 taxa
378 were identified, largely dominated by *Assulina muscorum* Greeff, *Corythion dubium*
379 Taranek, *Cryptodifflugia minuta* Playfair, *Cryptodifflugia oviformis* Penard,
380 *Trigonopyxis arcula* Penard, *Trinema lineare* Penard and *Valkanovia delicatula*
381 Valkanov. Poor preservation of testate amoebae is often observed in (poor-) fen peat
382 deposits due to high decomposition rates (Payne, 2011). Given this, it is impossible
383 to infer water table depth based upon the testate amoebae assemblages in the SSX
384 peat profile. Overall, the species composition of testate amoebae in the top layers of
385 the deposits resemble those identified in dry, poor fens (Opravilová and Hájek,
386 2006).

387

388 Representative I_D/I_G ratios and stacked first order Raman spectra are presented in
389 Figures 3 and 4, respectively. There is a distinct narrowing of the G band and
390 increase of the D band widths and intensity (height) (and thus increase of D band
391 area) in three of the samples compared to the others (206 cm, zone SSX-1; 101 cm,
392 zone SSX-2; 16 cm, zone SSX-5). These samples exhibit the greatest I_D/I_G ratios.

393

394 The TGA results (Fig. 5) highlight a distinct change in the quantity of the different OM
395 fractions (Capel et al., 2006) at ~103.5 cm (~ 7020 cal yr BP). All three OM fractions
396 increase at 103.5 cm (sample mid-point depth) with the most significant increases
397 observed in the recalcitrant and refractory fractions increasing by ~50% and ~66%
398 respectively.

399

400 The SSX carbon stable-isotope profile records an overall depth trend towards lower
401 $\delta^{13}C$ values (Fig. 5) which indicates that accumulation of recalcitrant material
402 depleted in ^{13}C dominates the isotopic profile (Alewell et al., 2011). Changes in $\delta^{13}C$
403 values along the peat profile are likely to reflect botanical changes to the peat
404 forming vegetation or changes in the extent of decomposition often related to
405 changes in the water table (Nykänen et al., 2018). Four of the most depleted $\delta^{13}C$
406 values were recorded in zone SSX1 of the peat profile (at mid-point depths of 203.5,
407 178.5, 168.5 and 163.5 cm). This is likely to reflect the presence of *Carex* spp. in this
408 zone, as these sedges have been found to record relatively depleted $\delta^{13}C$ values
409 between -29.19 to -27.98 ‰ (Skrzypek et al., 2008). A change to relatively enriched
410 $\delta^{13}C$ (-26.81 ‰) occurs at 158.5 cm (~8840 cal yr BP). This may indicate a change in
411 the water chemistry of the peatland (Nykänen et al., 2018) from a poor fen (relatively
412 depleted $\delta^{13}C$) to a bog (relatively enriched $\delta^{13}C$). A second series of depleted $\delta^{13}C$
413 values were recorded between 103.5-53.5 cm (~7020-4600 cal yr BP), which
414 indicates lower local water table depths with higher rates of decomposition leading to

415 an increased accumulation of ^{13}C depleted compounds such as lignin or phenols
416 (Alewell et al., 2011).

417

418 *4 Discussion*

419

420 *4.1 Peatland development*

421

422 The initial peatland development at the SSX site is marked by the presence of
423 *Juncus scheuchzerioides* seeds. This rush is a primary colonizer of bare ground and
424 occurs near pool margins (Upson and Lewis, 2014). The preservation of the *Carex*
425 spp. nutlets was not good enough to allow species level identification, but all of the
426 current 13 *Carex* species in the Falkland Islands grow near standing water or in fen
427 areas (Upson and Lewis, 2014). Abundant leaves of *Sphagnum magellanicum* at the
428 top of the zone suggest that the poor-fen stage persisted until ~8840 cal yr BP, given
429 that this moss occurs in both poor fen (minerotrophic) and bog (acidic, ombrotrophic)
430 peatlands in the Northern/Southern Hemisphere (Kyrkjeeide et al., 2016). The poor-
431 fen zone (SSX-1) extends between ~11,550-8840 cal yr BP during the Southern
432 Hemisphere Early Holocene thermal maximum (11,500-8500 yr BP, Kilian and Lamy,
433 2012). Multi-proxy palaeoclimate data from Laguna Azul (52°S, 69°W) in south-
434 eastern Patagonia indicate higher precipitation (decreased strength of the SWW)
435 between 11,200-10,199 cal yr BP (Zolitschka et al., 2019). Aeolian sand influx data
436 generated from a peat profile recovered from Isla de los Estados (55°S, 64°W) offers
437 evidence for decreased wind speeds between 12,200-10,000 cal yr BP (Björck et al.,
438 2012). In combination with higher precipitation, the reduced exposure to surface
439 winds may have favoured the initial (semi-) aquatic stages of the initial peatland
440 development. The SSX peatland would not have not been solely rainfed for the first
441 ~3000 years of peat accumulation, so it is not possible to generate a SWW climate
442 reconstruction for this section of the peat profile.

443

444 The peat stratigraphy in zones SSX-2 to -4 is relatively homogeneous and indicates
445 the presence of a stable grass bog between ~8840 to ~2820 cal yr BP, which was
446 frequently disturbed by fires. This matches the results recorded for xeric habitats in
447 the steppe-forest ecotone of Patagonia, as these sites also record high fire activity
448 throughout the Holocene (Huber et al., 2004). Preserved grass epidermis tissues
449 were not present, although it is likely that the undifferentiated graminoid and
450 graminoid roots remains are those of *Cortaderia pilosa*. During this long
451 'ombrotrophic' grass bog stage spanning ~6020 years, it is very difficult to detect
452 changes in mire surface wetness with the plant macrofossil data, given that
453 *Cortaderia pilosa* displays phenotypic plasticity, with a lax morphotype in poorly
454 drained peat and a tussock growth habit in well drained and sheltered areas
455 (Poskuta et al., 1998). The presence of trace amounts of *Sphagnum fimbriatum*
456 leaves in zones SSX-3 and -2 indicates the occurrence of some nutrient 'flushing',
457 given that this minerotrophic species (which has a bipolar global distribution) can
458 grow in moderately calcareous waters (Clymo and Hayward 1982) and is not
459 desiccation tolerant (Green 1968).

460

461 In Zone SSX-3 (~6590-5470 cal yr BP) there is a marked reduction in the numbers of
462 charcoal fragments in addition to high numbers of *Cennococcum geophilum* Fr.
463 sclerotia between 86-71 cm (~6250-5580 cal yr BP) and the highest recorded values
464 of *Myrteola nummularia* stems and undifferentiated Ericaceae wood. The increased
465 presence of dwarf shrubs in SSX-3 may be due to the reduced incidence of fires,
466 given that *Empetrum*-dominated ecosystems seem to have low resistance/resilience
467 to fire (Bråthen et al., 2010) possibly due to the sorptive properties of charcoal, which
468 reduce the allelopathic effects of dwarf shrub phenolic compounds (Wardle et al.,
469 1998; Keech et al., 2005). *C. geophilum* (species complex) is a globally ubiquitous
470 ectomycorrhizal fungi (Obase et al., 2017) with 129 species/variations/hybrids of host

471 plants which includes Myrtaceae (Trappe, 1964). *M. nummularia* (Myrtaceae) may
472 have therefore acted as the host plant for *C. geophilum* and its ectomycorrhizae may
473 have served to enhance water uptake by this dwarf shrub (Hasselquist et al., 2005).
474 *C. geophilum* appears to be relatively drought tolerant (Piggot, 1982; Coleman et al.,
475 1989) and its sclerotia can survive long-lasting drought treatments (Glassman et al.,
476 2015; Miyamoto and Nara 2016). Collectively, the macrofossil taxa in zone SSX3
477 therefore suggest that local water tables depths were relatively low, possibly as a
478 response to increased strength of the SWW (higher rates of evapotranspiration and
479 reduced precipitation, due to the negative correlation between 850-hPa zonal wind
480 speed strength and precipitation in eastern Patagonia (Garreaud et al., 2013)).

481

482 In the following zone (SSX-4, ~5470-2820 cal yr BP), *C. geophilum* sclerotia,
483 Ericaceae wood and *M. nummularia* all decrease, which may indicate shallower local
484 water table depths, possibly due to a weakening of the SWW. The most decayed
485 peat matrices (high percentages of unidentifiable organic material) occur in the
486 topmost zone (SSX-5, ~2820 cal yr BP to the present), combined with relatively high
487 amounts of Ericales rootlets. This may indicate another period of low local water
488 tables possibly due to increased SWW strength, impacts of European colonists
489 (Armstrong, 1994) from the eighteenth century to the present (grazing by cattle and
490 sheep), stratospheric ozone depletion over Antarctica (Fogt et al., 2009) or a
491 combination of these factors. Grazing in the Falkland Islands has reduced biomass
492 height, favoured *Empetrum rubrum* over *Cortaderia pilosa*, exposed more bare peat
493 surface, and perhaps also led to increased peat drying due to surface wind exposure.
494 There is a sustained presence of relatively high numbers of macrofossil charcoal
495 fragments and leaves of *Campylopus pyriformis* are present in zone SSX-5. This
496 bryophyte is an early coloniser on burnt peat surfaces (Thomas et al., 1994).

497

498 *4.2 Fire Regime*

499

500 With the exception of the surface sample (1cm depth), all of the other samples
501 contained large amounts of macrofossil charcoal fragments which indicate local
502 burning. This contrasts markedly with Thomas et al. (2018), where little/no fire was
503 detected in the local environment of the Canopus Hill peat profile, outside Stanley
504 (based upon micro-charcoal analyses), ~80 km to the east of the SSX peat profile.
505 There may therefore either be a high degree of spatial variability of wildfires in the
506 Falkland Islands, for example due to rainfall gradients (average rainfall is higher in
507 the east, which could have reduced fire frequency at the Canopus Hill site).
508 Alternatively, local burning may not have been detected in the study of Thomas et al.
509 (2018) because macro-charcoal analyses were not undertaken.

510

511 The plant macrofossil record indicates that the highest degree of mire surface
512 wetness occurred in zone SSX1, yet despite this, every sample contained large
513 numbers of macrofossil charcoal fragments. Moisture content of organic soils is the
514 single most important property governing the ignition and spread of smouldering peat
515 fires (Rein et al., 2008). One explanation for this is that the SSX peat profile dried out
516 seasonally during this time period, as this would have reduced the moisture content
517 of the above ground fine fuels, making them more likely to burn following lightning
518 strike induced ignition. Lightning activity is low (<0.01 strikes $\text{km}^{-2}\text{yr}^{-1}$) south of 40°S
519 along the Southern Hemisphere storm track (Virts et al., 2013), but between
520 (~11,550-8840 cal yr BP) enough strikes must have occurred to initiate local burning
521 of the peat bog vegetation. Hunter-gatherers have occupied southern continental
522 Patagonia and Northern Tierra del Fuego since ~11,000 years BP (Miotti et al., 2003;
523 Paunero, 2003; Massone and Prieto, 2004), but the earliest evidence for maritime
524 hunter-gatherer (shell middens) in southern South America currently only extends to
525 6500 ^{14}C years (Legoupil and Fontugne 1997). Given this, it is unlikely that there
526 could be a human cause for the burning registered in the SSX-1 peat profile, as the

527 timespan of zone SSX-1 predates by millennia the development of seaworthy craft by
528 the 'canoe people' (Alacalufe/Kaweskar and Yamana/Yagan), who were skilled
529 navigators and hunted pinnipeds using bark canoes (Morello et al., 2012).

530

531 The Raman spectroscopy suggests that the highest intensity fires (indicated by the
532 I_D/I_G ratios and more prominent D bands) occurred in zone SSX-1 at 206 cm, in zone
533 SSX-2 at 101 cm and in zone SSX-5 at 16 cm (Figs. 3 and 4). These higher intensity
534 fires may reflect a combination of favourable fire weather, low fuel moisture contents
535 and for SSX-5, possible human factors (deliberate burning of white grass peatlands)
536 although the likelihood of deliberate fires prior to European settlement in the 1760s
537 CE must be considered low. The highest intensity fires recorded by the Raman
538 spectroscopy at the base of zone SSX-1 may have also resulted from the fuel
539 structure in this section of the peat profile (*J. scheuchzerioides* is only present in
540 SSX-1) during the poor fen stage of peat accumulation. The remaining fires in zones
541 SSX-1 at 181 cm, SSX-2 at 131 cm, SSX-3 at 76 cm and SSX-4 at 46 cm all record
542 relatively lower intensity peat fires. The composition of the peat forming plants and
543 fungi in zone SSX-3 is anomalous and indicates relatively low peat water tables. In
544 northern Patagonia, fire occurrence and spread are promoted by droughts during the
545 fire season (October to April) and also appear to be favoured by above-average
546 moisture conditions during the preceding one to two growing seasons which
547 enhances flammable biomass production (Kitzberger et al., 1997). Low water tables
548 in zone SSX-3 between ~ 6590-5470 cal yr BP may have therefore prevented the
549 build-up of above-ground fine fuels, reducing the intensity of the resulting peat fires.
550 This is supported by the relatively low Raman I_D/I_G ratios for the sample at 76 cm
551 depth at ~5820 cal yr BP (Fig. 3).

552

553 *4.3 Changes in the strength of the Southern Westerly Winds?*

554

555 Detecting water table depth changes as a surrogate for changes in the strength of
556 the Southern Westerly Winds in the grass bog (rain-fed) sections of the SSX peat
557 profile (zones SSX-2 to -4, ~8840 to ~2820 cal yr BP) is difficult due to the poor
558 preservation of the testate amoeba assemblages. However, the increased values of
559 the TGA derived recalcitrant and refractory material in the peat profile (Fig. 5) from
560 ~103.5-53.5 cm (~7020-4600 cal yr BP) and depleted $\delta^{13}\text{C}$ values between the same
561 depth interval, suggest that the amount of effective precipitation was reduced from
562 ~7020 cal yr BP, as this is evidence for enhanced peat decay. This could be due to a
563 stronger drying effect of winds and reduced precipitation, given the negative
564 correlation between 850-hPa zonal wind speed strength and precipitation in eastern
565 Patagonia (Garreaud et al., 2013). This also ties in with the results of Saunders et al.
566 (2018) and Fernández et al. (2020) who also found evidence for enhanced Southern
567 Westerly wind strength from ~7000 cal yr BP and ~7250 cal yr BP, respectively. The
568 recalcitrant peat fractions record pronounced changes between (~7020-4600 cal yr
569 BP), which may indicate high variability of the effective precipitation during this time
570 period. The plant macrofossils in zone SSX-3 (6590-5470 cal yr BP) suggest low
571 mire surface wetness due to increased strength of the SWW. Björck et al. (2012)
572 identified two periods of higher wind speeds at 6400 and 5400 cal yr BP in Isla de los
573 Estados, Tierra del Fuego, based upon aeolian sand flux data. Mineral dust flux data
574 from Amsterdam Island record strengthened SWW at the northern edge of the
575 Southern Westerly wind belt (37°S) between 6200 to 4900 cal yr BP (Li et al., 2020).
576 Unfortunately, the quality of the SSX chronology does not match the Björck et al.
577 (2012) and Li et al. (2020) records, which weakens this Falkland Island 'evidence' for
578 SWW variability.

579 A compounding problem is the low long-term apparent rate of carbon accumulation in
580 the SSX peat profile. This was estimated to be $10.67 \text{ g C m}^{-2} \text{ yr}^{-1}$ (Payne et al. 2019),
581 which is <50% of the figure for the global mean accumulation rate of northern
582 peatlands (Loisel et al., 2014). This is likely to reflect a combination of low initial

583 carbon accumulation of the peat forming vegetation (due to the cool oceanic climate,
584 relatively low precipitation and high wind speeds) and subsequent losses of carbon
585 stocks due to the frequent occurrence of fires. Despite lying at the edge of the
586 climate envelope for global peatlands (Payne et al. 2019), the degree of recalcitrance
587 of Falkland Island peat matrices may well be high in order for peat to have
588 accumulated throughout the Holocene. The highly fibrous nature of *Cortaderia pilosa*
589 (Davies et al., 1990), which is the main Falkland Islands peat builder, may have
590 provided a degree of recalcitrance to the peat litter to permit continued carbon
591 sequestration (Scaife et al., 2019). In future work it would be interesting to measure
592 CO₂ net ecosystem exchange (NEE) fluxes for white grass peat in order to give
593 insight into their CO₂ sink strength.

594

595 *5 Conclusions*

596

597 The SSX peat profile has frequently burnt throughout the last ~11,500 years and
598 disturbance through burning is commonplace. This matches fire reconstructions from
599 xeric habitats of the steppe-forest ecotone in southern South America (Huber et al.
600 (2004). Raman spectroscopy builds upon the macrofossil data and offers additional
601 insight into the nature of former burning events which would otherwise be unknown.
602 Higher intensity fires may have occurred due to changes in the production of
603 flammable biomass (abundant fine fuels) due to higher rainfall under weaker SWW
604 winds (SSX-1). Higher intensity fires may also have occurred due to low peat
605 moisture under stronger SWW (recorded by the TGA data) at the top of zone SSX-2
606 and possible human factors (deliberate burning in zone SSX-5). The observed low
607 peat accumulation rates may have resulted from burning and the persistently low
608 annual precipitation the Falkland Islands received during the course of the Holocene.
609

610 The paucity of preserved tests of testate amoebae suggests that water table depths
611 in the grass bog peat profile are likely to have been too low to enable preservation of
612 these organisms. Given this, it is challenging to reconstruct changes in the strength
613 of the SWW using this technique. However, the results of the TGA and $\delta^{13}\text{C}$ analyses
614 suggest that a change in the strength of the SWW occurred around ~7020 cal yr BP
615 and that these methods have indicator value in slowly accumulating and fire-
616 disturbed peat profiles.

617

618 *Acknowledgments*

619

620 RJP secured funding for this research from the Quaternary Research Association,
621 University of York and the Russian Science Foundation (19-14-00102). We thank
622 Paul Brickle and other members of the South Atlantic Environmental Research
623 Institute for their help with logistics, David Large for valuable discussions about
624 Falkland Islands peat and all landowners for access permission. This work is
625 dedicated to Richard J. Payne who was tragically killed while climbing Peak 6477, a
626 previously unclimbed subsidiary peak of Nanda Devi (Garhwal Himalayas) in May
627 2019.

628

629 *References*

630

631 Aaby, B., Digerfeldt, G. 1986. Sampling Techniques for Lakes and Bogs. In:
632 Berglund, B.E., Ed., Handbook for Holocene Palaeoecology and Palaeohydrology,
633 John Wiley and Sons Ltd., Chichester, 181-194.

634

635 Alewell, C., Giesler, R., Klaminder, J., Leifeld, J., Rollog, M. 2011. Stable carbon
636 isotopes as indicators for environmental change in peatlands. *Biogeosciences* 8,
637 1769-1778.

638

639 Armstrong, P.H. 1994. Human impact on the Falkland Islands Environment. The
640 Environmentalist 14, 215-231.

641

642 Barrow, C. 1978. Postglacial pollen diagrams from south Georgia (sub-Antarctic) and
643 West Falkland island (South Atlantic). J. Biogeogr. 5, 251–274.

644

645 Bengtsson, L., Enell, M. 1986. Chemical analysis. In B.E. Berglund (Ed): Handbook
646 of Holocene Palaeoecology and Palaeohydrology, Wiley, Chichester, 423-445 p.

647

648 Bennett, K.D. 1996. Determination of the number of zones in a biostratigraphical
649 sequence. New Phytol. 132, 155-170.

650

651 Benscoter, B.W., Wieder, R.K. 2003. Variability in organic matter lost by combustion
652 in a boreal bog during the 2001 Chisholm fire. Can. J. For. Res. 33, 2509–2513.

653

654 Beyssac, O., Goffé, B., Chopin, C., Rouzaud, J.N. 2002. Raman spectra of
655 carbonaceous material in metasediments: A new geothermometer. J. Metamorph.
656 Geol. 20, 859–871.

657

658 Björck, S., Rundgren, M., Ljung, K., Unkel, I., Wallin, A. 2012. Multi-proxy analyses of
659 a peat bog on Isla de los Estados, easternmost Tierra del Fuego: a unique record of
660 the variable Southern Hemisphere Westerlies since the last deglaciation. Quaternary
661 Sci. Rev. 42, 1-14.

662

663 Blaauw, M., Christén, J.A. 2011. Flexible paleoclimate age- depth models using an
664 autoregressive gamma process. Bayesian Anal. 6, 457–474.

665

666 Blackford, J.J. 2000. Charcoal fragments in surface samples following a fire and the
667 implications for interpretation of subfossil charcoal data. *Palaeogeogr. Palaeocl.* 164,
668 33–42.

669

670 Bourgeau-Chavez, L.L., Grelik, S.L., Billmire, M., Jenkins, L.K., Kasischke, E.S.,
671 Turetsky, M.R. 2020. Assessing boreal peat fire severity and vulnerability of
672 peatlands to early season wildland fire. *Front. For. Glob. Change* 3, doi:
673 10.3389/ffgc.2020.00020.

674

675 Bråthen, K.A., Fodstad, C.H., Gallet, C. 2010. Ecosystem disturbance reduces the
676 allelopathic effects of *Empetrum hermaphroditum* humus on tundra plants. *J. Veg.*
677 *Sci.* 21, 786-795.

678

679 Brolly, C., Parnell, J., Bowden, S. 2016. Raman spectroscopy: caution when
680 interpreting organic carbon from oxidizing environments. *Planet. Space Sci.* 121, 53–
681 59.

682

683 Buckland, P. C., Edwards, K. J. 1998. Palaeoecological evidence for possible Pre-
684 European settlement in the Falkland Islands. *J. Archaeol. Sci.* 25, 599–602.

685

686 Capel, E.L., de la Rosa Arranz, J.M., González-Vila, F.J., González-Perez, J.A.,
687 Manning, D.A. 2006. Elucidation of different forms of organic carbon in marine
688 sediments from the Atlantic coast of Spain using thermal analysis coupled to isotope
689 ratio and quadrupole mass spectrometry. *Org. Geochem.* 37, 1983-1994.

690

691 Chambers, F.M., Booth, R.K., De Vleeschouwer, F., Lamentowicz, M., Le Roux,
692 G.G., Mauquoy, D., Nichols, J.E., van Geel, B., 2012. Development and refinement
693 of proxy-climate indicators from peats. *Quat. Int.* 268, 21–33.

694 <https://doi.org/10.1016/j.quaint.2011.04.039>.

695

696 Clark, J.S. 1988. Particle motion and the theory of charcoal analysis: source area,
697 transport, deposition, and sampling. *Quaternary Res.* 30, 67–80.

698

699 Clark, J.S., Lynch, J.A., Stocks, B.J., Goldammer, J.G. 1998. Relationships between
700 charcoal particles in air and sediments in west-central Siberia. *Holocene* 8, 19–29.

701

702 Clark, R., Huber, U.M., Wilson, P. 1998. Late Pleistocene sediments and
703 environmental change at Plaza Creek, Falkland Islands, South Atlantic. *J.*

704 *Quaternary Sci.* 13, 95-105.

705

706 Clymo, R.S., Hayward, P.M. 1982. The ecology of *Sphagnum*. In *Bryophyte ecology*.
707 Edited by A. J. E. Smith. Chapman and Hall, London. pp. 229-289.

708

709 Coleman, M.D., Bledsoe, C.S., Lopushinsky, W. 1989. Pure culture response of
710 ectomycorrhizal fungi to imposed water stress. *Can. J. Botany* 67, 29–39.

711

712 Davies, A.B., Riley, J., Walton, D.W.H. 1990. Plant form, tiller dynamics and above-
713 ground standing crops of the range of *Cortaderia pilosa* communities in the Falkland

714 Islands. *J. Appl. Ecol.* 27, 298-307.

715

716 Dean, J.W.E. 1974. Determination of carbonate and organic matter in calcareous
717 sediments and sedimentary rocks by loss on ignition: comparison with other

718 methods. *J. Sediment. Petrol.* 44, 242-248.

719

720 Fernández, M., Ponce, J.F., Ramón Mercau, J., Coronato, A., Laprida, C., Maidana,
721 N., Quiroga, D., Magneres, I. 2020. Paleolimnological response to climate variability

722 during Late Glacial and Holocene times: A record from Lake Arturo, located in the
723 Fuegian steppe, southern Argentina. *Palaeogeogr. Palaeoclimatol. Palaeoecol.*,
724 <https://doi.org/10.1016/j.palaeo.2020.109737>
725
726 Ferrari, A.C., Robertson, J. 2001. Resonant Raman spectroscopy of disordered,
727 amorphous and diamond-like carbon. *Phys. Rev. B* 64, 075414.
728
729 Fogt, R.L., Perlwitz, J., Monaghan, A.J., Bromwich, D.H., Jones, J.M., Marshall, G.J.
730 2009. Historical SAM variability. Part II: Twentieth-Century variability and trends from
731 reconstructions, observations, and the IPCC AR4 models. *J. Climate* 22, 5346–5365.
732
733 Garreaud R., Lopez P., Minvielle M., Rojas, M. 2013. Large-scale control on the
734 Patagonian climate. *J. Climate* 26, 215–230.
735
736 Glassman, S.I., Peay, K.G., Talbot, J.M., Smith, D.P., Chung, J.A., Taylor, J.W.,
737 Vilgalys, R., Bruns, T.D. 2015. A continental view of pine-associated ectomycorrhizal
738 fungal spore banks: a quiescent functional guild with a strong biogeographic pattern.
739 *New Phytol.* 205, 1619–1631.
740
741 Green, B. H. 1968. Factors influencing the spatial and temporal distribution of
742 *Sphagnum imbricatum* Homsch. ex Russ. in the British Isles. *J. Ecol.* 56, 47-58.
743
744 Gregorich, E.G., Gillespie, A.W., Beare, M.H., Curtin, D., Sanei, H., Yanni, S.F. 2015.
745 Evaluating biodegradability of soil organic matter by its thermal stability and chemical
746 composition. *Soil Biol. Biochem.* 91, 182–191.
747

748 Hasselquist N., Germino M.J., McGonigle T., Smith W.K. 2005. Variability of
749 *Cenococcum* colonization and its ecophysiological significance for young conifers at
750 alpine-treeline. *New Phytol.* 165, 867–873.
751
752 Heusser, C.J. 1995. Three late Quaternary pollen diagrams from Southern Patagonia
753 and their palaeoecological implications. *Palaeogeogr. Palaeoclimatol.* 118, 1-24.
754
755 Hogg A.G., Hua Q., Blackwell P.G., Niu, M., Buck, C.E., Guilderson, T.P., Heaton,
756 T.J., Palmer, J.G., Reimer, P.J., Reimer, R.W., Turney, C.S.M., Zimmerman, S.R.H.
757 2013. SHCal13 Southern Hemisphere calibration, 0–50,000 years cal BP.
758 *Radiocarbon* 55, 1889-1903.
759
760 Hooker, J.D. 1847. The botany of the Antarctic voyage of H.M. Discovery Ships
761 Erebus and Terror in the Years 1839-1843. Under the command of Captain Sir
762 James Clark Ross. Reeve Brothers, London.
763
764 Huber, U.M., Markgraf, V., Schäbitz, F. 2004. Geographical and temporal trends in
765 Late Quaternary fire histories of Fuego-Patagonia, South America. *Quaternary Sci.*
766 *Rev.* 23, 1079-1097.
767
768 Hughes, P.D.M., Mauquoy, D., Barber, K.E., Langdon, P.G. 2000. Mire-development
769 pathways and palaeoclimatic records from a full Holocene peat archive at Walton
770 Moss, Cumbria, England. *Holocene* 10, 465–479.
771
772 Inoue, Yoshie, A., Tanaka, T., Onji, T., Inoue, Y. 2017. Disappearance and alteration
773 process of charcoal fragments in cumulative soils studied using Raman
774 spectroscopy. *Geoderma* 285, 164-172.
775

776 Jehlička, J. and Bény, C. 1992. Application of Raman microspectrometry in the study
777 of structural changes in Precambrian kerogens during regional metamorphism. *Org.*
778 *Geochem.* 18, 211–213.
779

780 Jones, P.D., Harpham, C., Lister, D. 2016. Long-term trends in gale days and
781 storminess for the Falkland Islands. *Int. J. Climatol.* 36, 1413-1427.
782

783 Keech, O., Carcaillet, C., Nilsson, M.C. 2005. Adsorption of allelopathic compounds
784 by wood-derived charcoal: the role of wood porosity. *Plant Soil* 272, 291–300.
785

786 Kilian, R., Lamy, F. 2012. A review of Glacial and Holocene paleoclimate records
787 from southernmost Patagonia (49-55°S). *Quaternary Sci. Rev.* 53, 1-23.
788

789 Kitzberger, T., Veblen, T.T., Villalba, R. 1997. Climatic influences on fire regimes
790 along a rain forest-to-xeric woodland gradient in northern Patagonia, Argentina. *J.*
791 *Biogeogr.* 24, 35-47.
792

793 Knight, D.S., White, W.B. 1989. Characterization of diamond films by Raman
794 spectroscopy. *J. Mater. Res.* 4, 385–393.
795

796 Kristensen, E., 1990. Characterization of biogenic organic matter by stepwise
797 thermogravimetry (STG). *Biogeochemistry* 9,135-159.
798

799 Kuhry, P. 1994. The role of fire in the development of *Sphagnum*-dominated
800 peatlands in western boreal Canada. *J. Ecol.* 82, 899-910.
801

802 Kyrkjeeide, M. O., Hassel, K., Flatberg, K.I., Shaw, A.J., Yousefi, N., Stenøien, H.K.
803 2016. Spatial Genetic Structure of the Abundant and Widespread Peatmoss

804 *Sphagnum magellanicum* Brid. PLoS ONE 1111: e0148447. doi:10.1371/journal.
805 pone.0148447</Info
806
807 Landis C.A. 1971. Graphitisation of dispersed carbonaceous material in metamorphic
808 rocks. Contrib. Mineral. Petr. 30, 34-45.
809
810 Legoupil, D., Fontugne, R. 1997. El poblamiento marítimo en los archipiélagos de
811 Patagonia: núcleos antiguos y dispersión reciente. Anales del Instituto de la
812 Patagonia. Serie Ciencias Humanas 25, 75-87.
813
814 Li, C., Sonke, J.E., Le Roux, G., Van der Putten, N., Piotrowska, N., Jeandel, C.,
815 Mattielli, N., Benoit, M., Wiggs, G.S.F., De Vleeschouwer, F. 2020. Holocene
816 dynamics of the southern westerly winds over the Indian Ocean inferred from a peat
817 dust deposition record. Quat. Sci. Rev. 231,
818 <https://doi.org/10.1016/j.quascirev.2020.106169>
819
820 Loisel, J., Yu, Z., Beilman, D.W., Camill, P., Alm, J., Amesbury, M.J., Anderson, D.,
821 Andersson, S., Bochicchio, C., Barber, K., Belyea, L.R., Bunbury, J., Chambers,
822 F.M., Charman, D.J., De Vleeschouwer, F., Fiałkiewicz-Kozieł, B., Finkelstein, S.A.,
823 Gałka, M., Garneau, M., Hammarlund, D., Hinchcliffe, W., Holmquist, J., Hughes, P.,
824 Jones, Klein, E.S., Kokfelt, U., Korhola, A., Kuhry, P., Lamarre, A., Lamentowicz, M.,
825 Large, D., Lavoie, M., MacDonald, G., Magnan, G., Mäkilä, M., Mallon, G.,
826 Mathijssen, P., Mauquoy, D., McCarroll, J., Moore, T.R., Nichols, J., O'Reilly, B.,
827 Oksanen, P., Packalen, M., Peteet, D., Richard, P.J.H., Robinson, S., Ronkainen, T.,
828 Rundgren, M., Sannel, A.B.K., Tarnocai, C., Thom, T., Tuittila, E.-S., Turetsky, M.,
829 Väiliranta, M., van der Linden, M., van Geel, B., van Bellen, S., Vitt, D., Zhao, Y.,
830 Zhou, W. 2014. A database and synthesis of northern peatland soil properties and
831 Holocene carbon and nitrogen accumulation. Holocene 24, 1028-1042.

832

833 Loisel, J., Yu, Z. 2013. Holocene peatland carbon dynamics in Patagonia.

834 Quaternary Sci. Rev. 69, 125-141.

835

836 Lopez-Capel, E., Sohi, S.P., Gaunt, J.L., Manning, D.A. 2005. Use of

837 thermogravimetry–differential scanning calorimetry to characterize modelable soil

838 organic matter fractions. Soil Sci. Soc. Am. J. 69, 136-140.

839

840 Mariani, M., Holz, A., Veblen, T.T., Williamson, G., Fletcher, M.-S., Bowman,

841 D.M.J.S. 2018. Climate change amplifications of climate-fire teleconnections in the

842 Southern Hemisphere. Geophys. Res. Lett. 45, [https://doi.org/10.1029/](https://doi.org/10.1029/2018GL078294)

843 2018GL078294.

844

845 Massone, M., Prieto, A. 2004. Evaluación de la Modalidad Cultural Fell 1 en

846 Magallanes. Chungará 36 (suppl.): 303–315.

847

848 Mazei, Y.A., Chernyshov, V.A. 2011. Testate amoebae communities in the southern

849 tundra and forest-tundra of Western Siberia. Biology Bull. 38, 789–796.

850

851 McAdam, J.H., Upson, R. 2012. Peatlands in the Falkland Islands – Origins, status

852 and threats. IUCN UK Peatland Programme/British Ecological Society Symposium,

853 Bangor Wales. p15.

854

855 Michaelis, D. 2011. Die *Sphagnum*-Arten der Welt. Bibliotheca Botanica 160,

856 Schweizerbart Science Publishers, Stuttgart, 408 pp. (in German).

857

858 Miotti, L., Salemme, M., Rabassa, J. 2003. Radiocarbon chronology at Piedra Museo

859 locality. In: Miotti, L., Salemme, M., Flegenheimer, N. (Eds.), Where the South Winds

860 Blow. Centre for the Study of First Americans and Texas A and M University Press,
861 Texas, 99-104.
862

863 Miyamoto, Y., Nara, K. 2016. Soil propagule banks of ectomycorrhizal fungi share
864 many common species along an elevation gradient. *Mycorrhiza* 26, 189–197.
865

866 Morello, F., Borrero, L., Massone, M., Stern, C., García-Herbst, A., McCulloch, R.,
867 Arroyo-Kalin, M., Calás, E., Torres, J., Prieto, A., Martinez, I., Bahamonde, G.,
868 Cárdenas, P. 2012. Hunter-gatherers, biogeographic barriers and the development of
869 human settlement in Tierra del Fuego. *Antiquity* 86, 71-87
870

871 Muirhead, D.K., Parnell, J., Taylor, C., Bowden, S.A. 2012. A kinetic model for the
872 thermal evolution of sedimentary and meteoritic organic carbon using Raman
873 spectroscopy. *J. Anal. Appl. Pyrol.* 96, 153–161.
874

875 Muirhead, D.K., Parnell, J., Spinks, S., Bowden, S.A. 2017. Characterization of
876 organic matter in the Torridonian using Raman spectroscopy. *Geol. Soc. Spec. Publ.*
877 448, 71-80.
878

879 Muirhead, D.K., Bond, C.E., Watkins, H., Butler, R.W., Schito, A., Crawford, Z. and
880 Marpino, A. 2019. Raman Spectroscopy: an effective thermal marker in low
881 temperature carbonaceous fold-thrust belts. *Geol. Soc. Spec. Publ.* 490, doi:
882 10.1144/SP490-2019-27.
883

884 Nemanich, R.J., Solin, S.A. 1979. First and second order Raman scattering from
885 finite-size crystals of graphite. *Phys. Rev. B*, 20, 392–401.
886

887 Nykänen, N., Mpamah, P.A., Rissanen, A.J. 2018. Stable carbon isotopic
888 composition of peat columns, subsoil and vegetation on natural and forestry drained
889 boreal peatlands. *Isot. Environ. Health*. S. 54, 622-641,
890 DOI:10.1080/10256016.2018.1523158.
891
892 Obase, K., Douhan, G.W., Matsuda, Y., Smith, M.E. 2017. Progress and Challenges
893 in Understanding the Biology, Diversity, and Biogeography of *Cenococcum*
894 *geophilum*. In: Tedersoo L. (eds) *Biogeography of Mycorrhizal Symbiosis*. *Ecological*
895 *Studies (Analysis and Synthesis)*, vol. 230. Springer, Cham.
896
897 Opravilová, V., Hájek, M. 2006. The variation of testacean assemblages (Rhizopoda)
898 along the complete base-richness gradient in fens: a case study from the western
899 Carpathians. *Acta Protozool.* 45, 191-204.
900
901 Pasteris J. D., Wopenka, B. 1991. Raman spectra of graphite as indicators of degree
902 of metamorphism. *Can. Mineral.* 29, 1-9.
903
904 Paunero, R., 2003. The Cerro Tres Tetras (C3T) locality in the central plateau of
905 Santa Cruz, Argentina. In: Miotti, L., Salemme, M., Flegenheimer, N. (Eds.), *Where*
906 *the South Winds Blow*. Centre for the Study of First Americans and Texas A and M
907 University Press, Texas, 133-140.
908
909 Payne, R.J. 2011. Can testate amoeba-based palaeohydrology be extended to fens?
910 *J. Quaternary Sci.* 26, 15–27.
911
912 Payne, R.J., Ring-Hrubesh, F., Rush, G., Sloan, T.J., Evans, C.D. and Mauquoy, D.
913 2019. Peatland initiation and carbon accumulation in the Falkland Islands.
914 *Quaternary Sci. Rev.* 212, 213-218.

915

916 Peters, M.E., Higuera, P.E. 2007. Quantifying the source area of macroscopic
917 charcoal with a particle dispersal model. *Quaternary Res.* 67, 304-310.

918

919 Piggott C.D. 1982. Survival of mycorrhiza formed by *Cenococcum geophilum* Fr. in
920 dry soils. *New Phytol.* 92, 513–517.

921

922 Piotrowska, N. 2013. Status report of AMS sample preparation laboratory at GADAM
923 Centre, Gliwice, Poland. *Nucl. Instrum. Methods Phys. Res. B* 294, 176-181.

924 <https://doi.org/10.1016/j.nimb.2012.05.017>

925

926 Pisaric, M.F.J. 2002. Long-distance transport of terrestrial plant material by
927 convection resulting from forest fires. *J. Paleolimnol.* 28, 349–354.

928

929 Plante, A. F., Fernandez, J. M., Leifeld, J. 2009. Application of thermal analysis
930 techniques in soil science. *Geoderma* 153, 1–10,

931 [doi:10.1016/j.geoderma.2009.08.016](https://doi.org/10.1016/j.geoderma.2009.08.016).

932

933 Poskuta, J.W., McAdam, J.H., Waclawczyk-Lach, E., Wróbleska, B. 1998.

934 Photosynthetic and Respiratory Characteristics of *Cortaderia pilosa* (D'Urv.) Hack.,
935 the Dominant Component of Falkland Islands. *J. Plant Physiol.* 153, 517-519.

936

937 Rein G., Cleaver N., Ashton C., Pironi P., Torero J. L. 2008. The severity of
938 smouldering peat fires and damage to the forest soil. *Catena* 74, 304-309.

939

940 Rosenheim B.E., Day, M.B., Domack, E., Schrum, H., Beenthien, A., Hayes, J.M.

941 2008. Antarctic sediment chronology by programmed-temperature pyrolysis:

942 methodology and data treatment. *Geochem. Geophys. Geosy.* 9,
943 doi:10.1029/2007GC001816.

944

945 Rosenheim, B.E., Galy, V. 2012. Direct measurement of riverine particulate organic
946 carbon age structure. *Geophys. Res. Lett.* 39, doi:10.1029/2012GL052883.

947

948 Rouzaud, J.N., Oberlin, A., Beny-Bassez, C. 1983. Carbon films: Structure and
949 microtexture (optical and electron microscopy, Raman spectroscopy). *Thin Solid*
950 *Films* 105, 75–96.

951

952 Saunders, K.M., Roberts, S.J., Perren, B., Butz, C., Sime, L., Davies, S., Van
953 Nieuwenhuyze, W., Grosjean, M., Hodgson, D.A. 2018. Holocene dynamics of the
954 Southern Hemisphere westerly winds and possible links to CO₂ outgassing. *Nat.*
955 *Geosci.* 11, 650-655.

956

957 Scaife, R.G., Long, A.J., Monteath, A.J., Hughes, P.D.M., Bentley, M.J., Stone, P.
958 2019. The Falkland Islands' palaeoecological response to millennial-scale climate
959 perturbations during the Pleistocene–Holocene transition: Implications for future
960 vegetation stability in the southern ocean islands. *J. Quaternary Sci.*, DOI:
961 10.1002/jqs.3150.

962

963 Schäbitz, F. 1991. Holocene vegetation and climate in southern Santa Cruz,
964 Argentina. *Bamberger Geographische Schriften* 11, 235-244.

965

966 Skrzypek, G., Paul, D., Wojtun, B. 2008. Stable isotope composition of plants and
967 peat from Arctic mire and geothermal area in Iceland. *Pol. Polar Res.* 29, 365–376.

968

969 Thomas, P.A., Proctor, M.C.F., Maltby, E. 1994. The ecology of severe moorland fire
970 on the North York Moors: chemical and physical constraints on moss establishment
971 from spores. *J. Ecol.* 82, 457-474.
972

973 Thomas, Z.A., Jones, R.T., Fogwill, C.J., Hatton, J., Williams, A.N., Hogg, A.,
974 Mooney, S., Jones, P., Lister, D., Mayewski, P., Turney, C.S.M. 2018. Evidence for
975 increased expression of the Amundsen Sea Low over the South Atlantic during the
976 late Holocene. *Clim. Past* 14, 1727-1738.
977

978 Tinner, W., Hofstetter, S., Zeugin, F., Conedera, M., Wohlgemuth, T., Zimmermann,
979 L., Zweifel, R. 2006. Long-distance transport of macroscopic charcoal by an intensive
980 crown fire in the Swiss Alps—implications for fire history reconstruction. *Holocene*
981 16, 287–292.
982

983 Trappe J.M. 1964. Mycorrhizal host and distribution of *Cenococcum graniforme*.
984 *Lloydia* 27, 100–106.
985

986 Tuinstra, F., Koenig, J.L. 1970. Raman spectrum of graphite. *Chem. Phys.* 53, 1126–
987 1130.
988

989 Turetsky, M.R., Donahue, W.F., Benscoter, B.W. 2011. Experimental drying
990 intensifies burning and carbon losses in a northern peatland. *Nat. Commun.* 2, doi:
991 10.1038/ncomms1523.
992

993 Turney C.S.M., Jones R.T., Fogwill C., Hatton, J., Williams, A.N., Hogg, A., Thomas,
994 Z.A., Palmer, J., Mooney, S., Reimer, R.W. 2016. A 250-year periodicity in Southern
995 Hemisphere westerly winds over the last 2600 years. *Clim. Past* 12, 189–200.
996

997 Upson R and Lewis R. 2014. Updated atlas and checklist. Report to Falklands
998 Conservation. 226 pp.
999

1000 van Bellen, S., Mauquoy, D., Hughes, P.D.M., Roland, T.P., Daley, T.J., Loader,
1001 N.J., Street-Perrott, F.A., Rice, E.M., Pancotto, V.A., Payne, R.J. 2016. Late-
1002 Holocene climate dynamics recorded in the peat bogs of Tierra del Fuego, South
1003 America. *Holocene* 26, 489-501.
1004

1005 Virts, K.S., Wallace, J.M., Hutchins, M.L., Holzworth, R.H. 2013. Highlights of a new
1006 ground-based, hourly global lightning climatology. *B. Am. Meteorol. Soc.* 94, 1381-
1007 1391.
1008

1009 Wardle, D.A., Zackrisson, O., Nilsson, M.C. 1998. The charcoal effect in boreal
1010 forests: mechanisms and ecological consequences. *Oecologia* 115, 419–426.
1011

1012 Wilson, P., Clark, R., Birnie, J., Moore, D.M. 2002. Late Pleistocene and Holocene
1013 landscape evolution and environmental change in the Lake Sullivan area, Falkland
1014 Islands, South Atlantic. *Quaternary Sci. Rev.* 21, 1821–1840.
1015

1016 Worrall, F., Moody, C.S., Clay, G.D., Burt, T.P., Rose, R., 2017. The flux of organic
1017 matter through a peatland ecosystem: The role of cellulose, lignin, and their control
1018 of the ecosystem oxidation state. *J. Geophys. Res.- Biogeo.* 122, 1655-1671.
1019

1020 Yamauchi, S., Kurimoto, Y. 2003. Raman spectroscopic study on pyrolyzed wood
1021 and bark of Japanese cedar: temperature dependence of Raman parameters. *J.*
1022 *Wood Sci.* 49, 235-240.
1023

- 1024 Zolitschka, B., Fey, M., Janssen, S., Maidana, N. I., Mayr, C., Wulf, S., Haberzettl, T.,
1025 Corbella, H., Lücke, A., Ohlendorf, C., Schäbitz, F. Southern Hemispheric Westerlies
1026 control sedimentary processes of Laguna Azul (south-eastern Patagonia, Argentina).
1027 *Holocene* 29, 402-420.
1028
1029

1030

Lab ID	Depth (cm)	¹⁴ C age (BP)	Sample composition	Calibrated age ranges (cal yr BP)	Modelled age (cal yr BP)
GdA-5971	21	2535±25	Charcoal fragments and above-ground graminoid leaf fragments	68.2% probability 2740 (39.7%) 2700 2630 (10.2%) 2620 2585 (4.5%) 2575 2560 (13.8%) 2540 95.4% probability 2740 (43.9%) 2690 2635 (12.6%) 2615 2590 (38.9%) 2500	2580±90
GdA-5972	71	4875±30	Fungal fruit bodies (<i>Cenococcum</i> spp. sclerotia)	68.2% probability 5640 (19.2%) 5630 5610 (49.0%) 5590 95.4% probability 5655 (95.4%) 5585	5585±100
GdA-5974	131	7365±30	Charcoal fragments and above-ground graminoid leaf fragments	68.2% probability 8300 (17.9%) 8260 8210 (38.2%) 8160 8110 (0.7%) 8120 8090 (11.5%) 8060 95.4% probability 8310 (95.4%) 8050	8170±90
GdA-5973	161	7885±30	<i>Sphagnum magellanicum</i> leaves, stems and branches	68.2% probability 8740 (3.2%) 8740 8720 (65.0%) 8600 95.4% probability 8970 (5.9%) 8920 8900 (1.1%) 8890 8860 (4.9%) 8830 8790 (83.5%) 8590	8850±120
D-AMS-029686	211	10,090±30	Above-ground graminoid leaf fragments	68.2% probability 11760 (65.7%) 11610 11520 (2.5%) 11510 95.4% probability 11930 (2.3%) 11890 11820 (76.6%) 11590 11570 (16.5%) 11410	11560±210

1031

1032

Table 1. Details and results of dated subsamples. Depth refers to the position of the

1033

centre of each subsample.

1034

1035

Macrofossil zone	Depth (cm)	Age (cal yr BP)	Main features
SSX-5	23.5-1 cm	2820-present	Marked increase in the percentage abundances of unidentifiable organic material, with peak values of 72% at 16 cm depth. Relatively high values of Ericales rootlets. The sample at 1 cm depth contains abundant <i>Campylopus pyriformis</i> leaves. Relatively high charcoal fragments between 16-6 cm. LOI decreases between 16-6 cm (86.5 to 83% respectively).
SSX-4	68.5-23.5 cm	5470-2820	Increase in the number of charcoal fragments with maxima at 61 cm and between 46-36 cm. Charcoal fragments decrease towards the top of the zone (31-26 cm). Ericales rootlets are consistently present between 46-26 cm.
SSX-3	93.5-68.5 cm	6590-5470	Marked reduction in the number of charcoal fragments. The highest numbers/percentages of <i>Cennococcum geophilum</i> , cf. Type 8 fruit bodies, <i>Myrteola nummularia</i> stems and Ericaceae wood were recorded in this zone.
SSX-2	158.5-93.5 cm	8840-6590	The peat matrices are dominated by undifferentiated graminoids and graminoid roots. Relatively high values of Ericales rootlets (~13%) were recorded at 151 cm. Sporadic presence of <i>Sphagnum fimbriatum</i> leaves (~1% only). Constant charcoal throughout, but the highest number occur between 141-121 cm. Reduced charcoal present between 116-106 cm.
SSX-1	211-158.5 cm	11,550-8840	Relatively low LOI values between 211-206 cm (55% and 67% respectively). High numbers of <i>Juncus scheuchzerioides</i> seeds at the base of the profile, followed by relatively high numbers of <i>Carex</i> spp. nutlets. High values (up to 84%) of <i>Sphagnum magellanicum</i> at the top of the zone. Relatively high numbers of charcoal fragments present between 206-201 cm and 186-181 cm. Reduced charcoal present between 176-161 cm.

1036

1037 Table 2 Macrofossil zonation for the SSX profile

1038

1039 Figure captions:

1040

1041 Fig. 1: **a.** location of the Falkland Islands/Islas Malvinas in the South Atlantic Ocean,
1042 **b.** site locations: Sussex Mountains (SSX, 58.99654°W, 51.63278°S) peat profile
1043 (black triangle), other sites mentioned in the text (black squares), Canopus Hill
1044 (Turney et al., 2016), Hooker's Point (Scaife et al., 2019), Lake Sullivan (Wilson et al.,
1045 2002), Sapper Hill (Buckland and Edwards (1998) **c.** photograph of the SSX peat
1046 profile coring location.

1047

1048 Fig. 2: Bacon age depth model. The accumulation rate prior was set to 50 years cm⁻¹
1049 with a shape of 1.5. The memory prior was set to a strength of 4 and a mean of 0.7.
1050 The model is based upon 43 sections (5 cm thick).

1051

1052 Fig. 3: SSX loss-on-ignition and plant macrofossils. Volume abundances of all
1053 components are expressed as percentages with the exception of seeds, nutlets,
1054 fungal fruit bodies/sclerotia and charcoal fragments, which are presented as the
1055 number (n) found in each ~ 5 cm³ subsample. The highest 3 Raman Intensity ratios
1056 (I_D/I_G) bars are filled with red, the remainder (lower I_D/I_G ratios) are filled with orange.
1057 The zonation is based upon the loss-on-ignition, plant macrofossil and macrofossil
1058 charcoal data.

1059

1060 Fig. 4: Raman scattering intensity vs. Raman shifts. D = disorder peak, G = graphite
1061 peak. The three highest intensity fires from the seven samples (at 206, 101 and 16
1062 cm depth) are filled with red, the remainder indicate lower intensity fires (filled with
1063 orange).

1064

1065 Fig. 5: $\delta^{13}\text{C}$ and TGA, OM mass loss data grouped into three thermal fractions: labile
1066 (200-400°C), recalcitrant (400-550°C) and refractory (550-650°C). The zonation is
1067 based upon the loss-on-ignition, plant macrofossil and macrofossil charcoal data.
1068

Figure 1

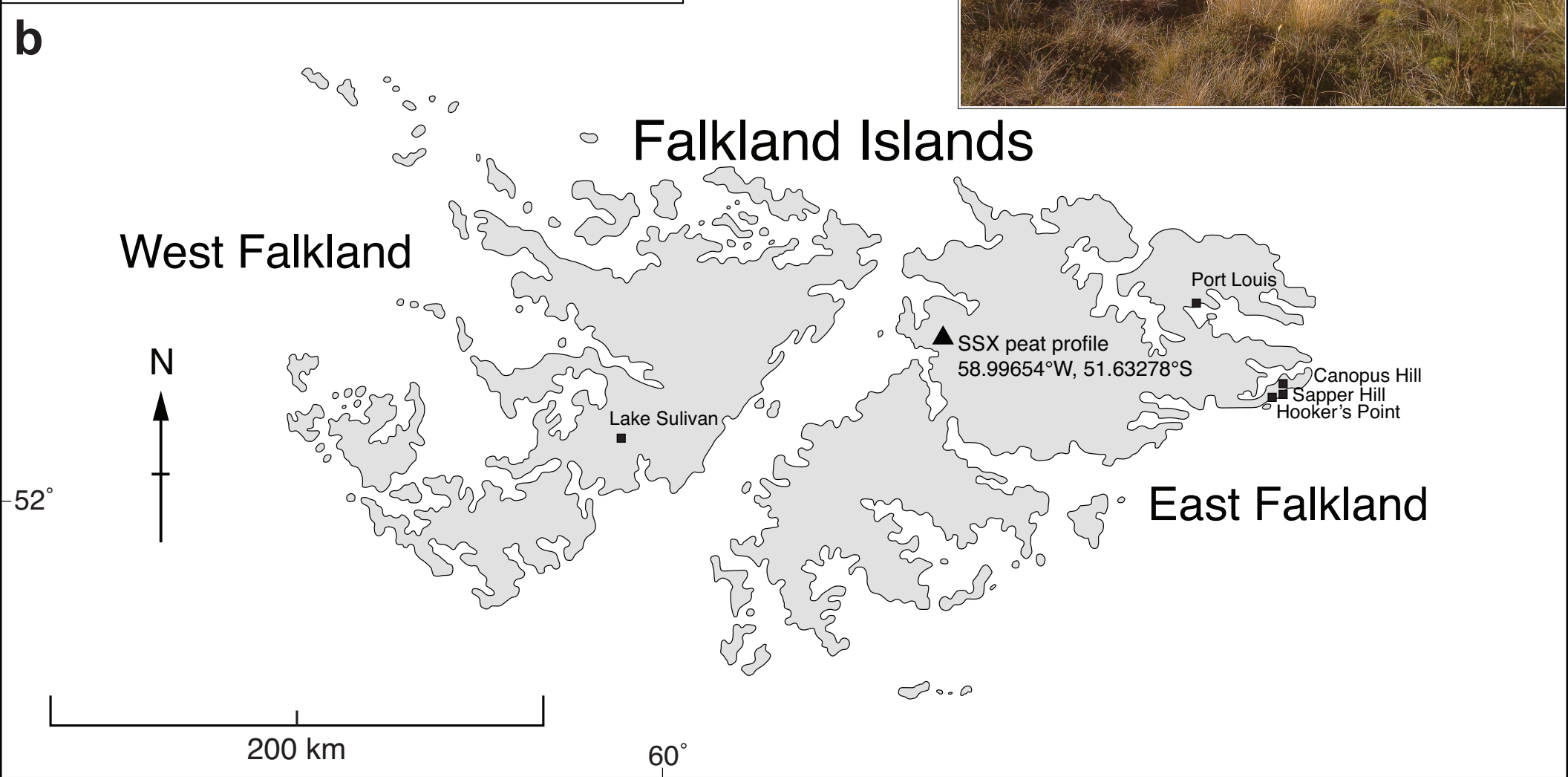
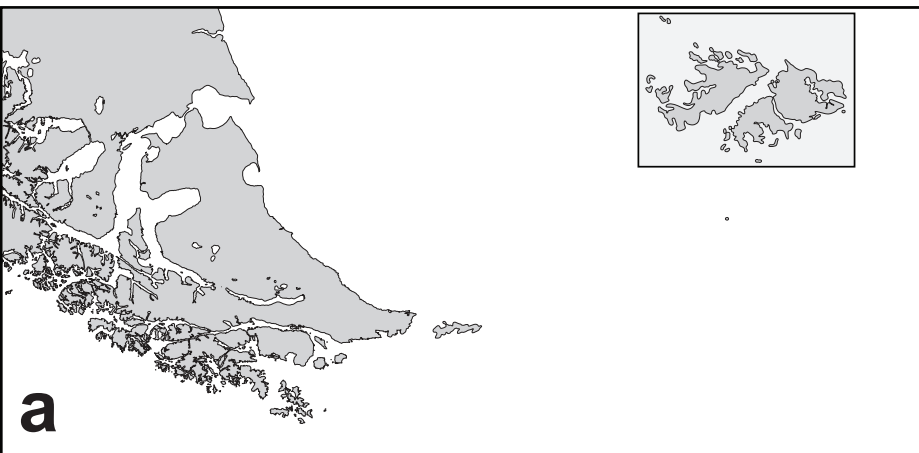


Figure 2

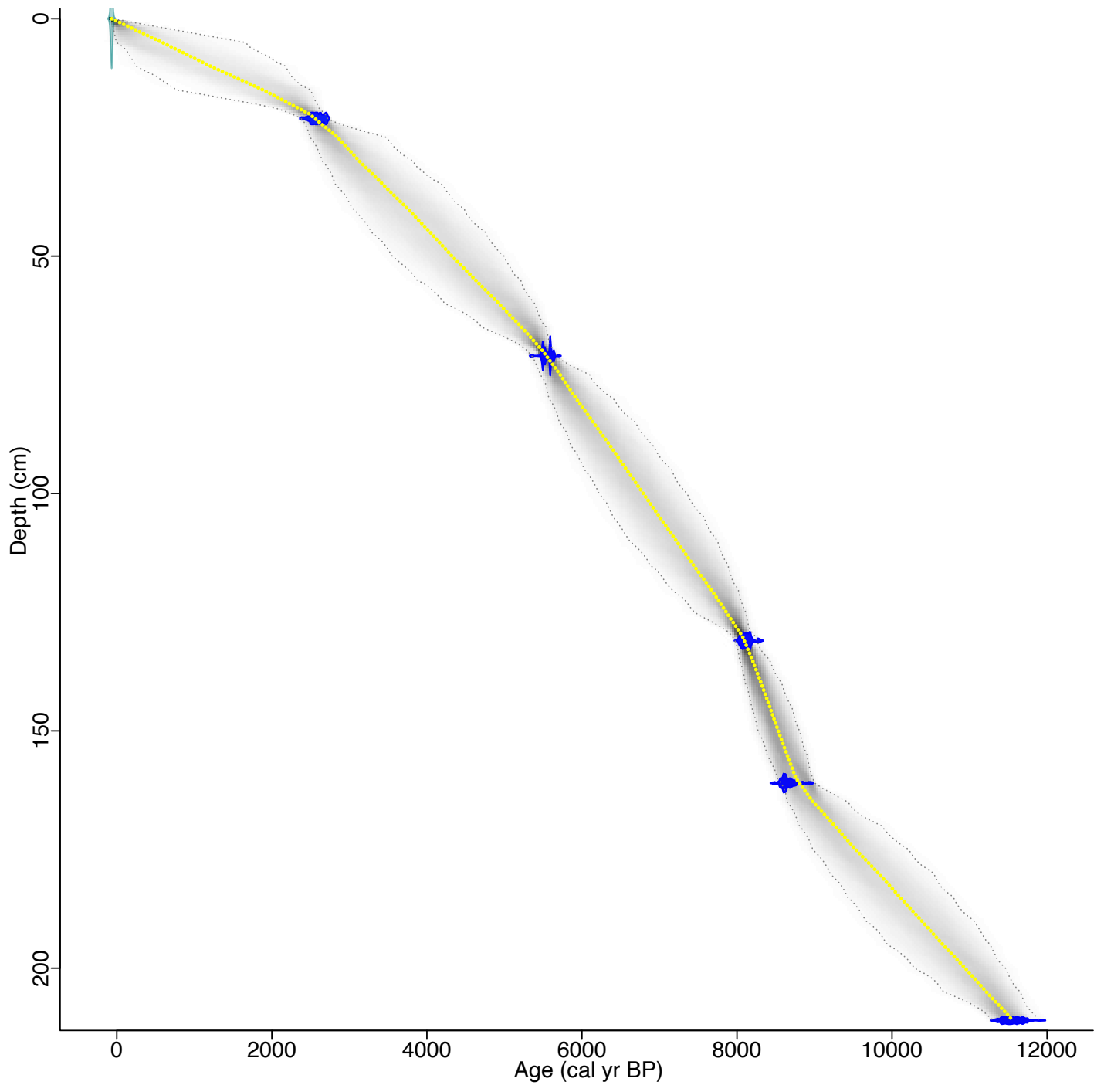


Figure 3

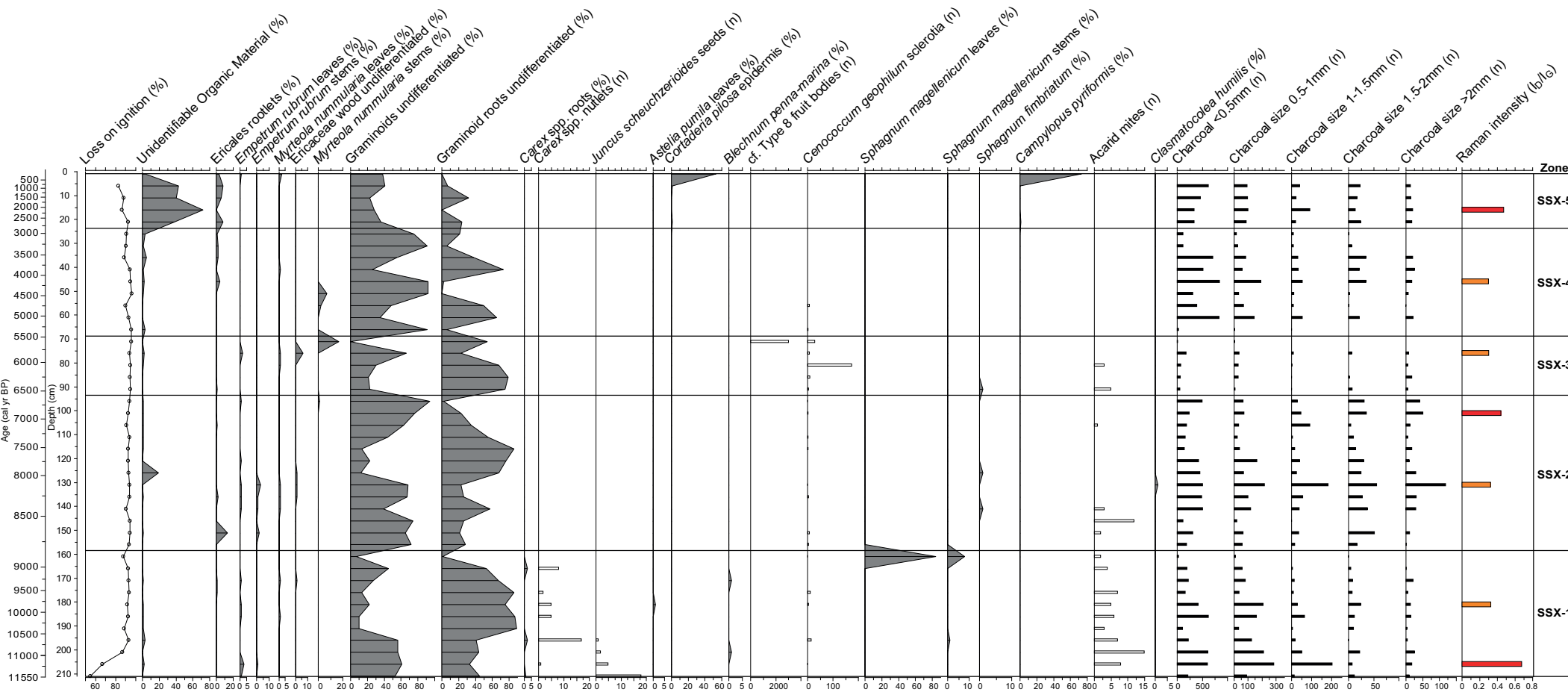


Figure 4

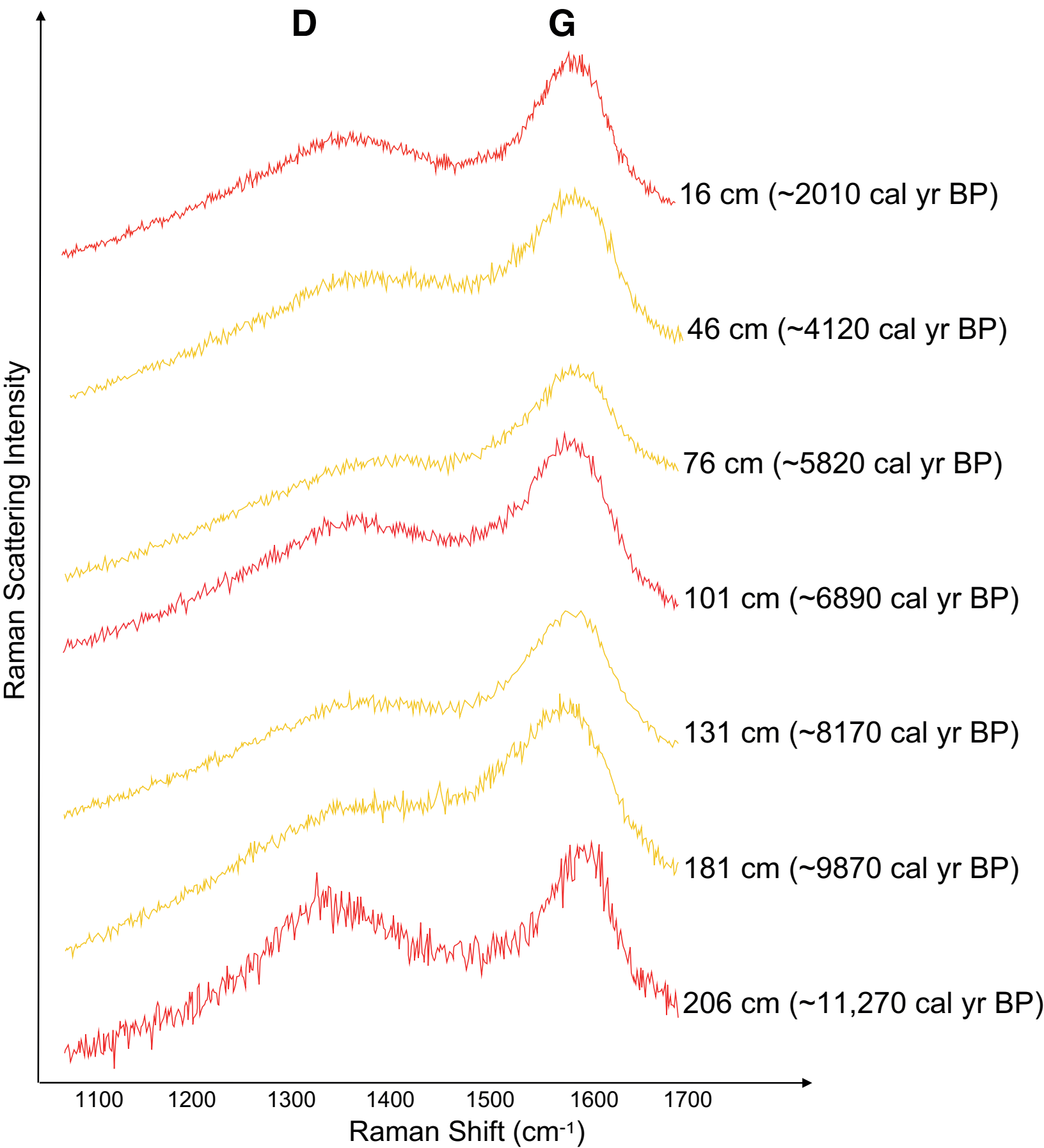


Figure 5

